Computational analysis and design formula development for the design of curved plates for ships and offshore structures

Joo-Hyun Kim[1], Joo-Shin Park[2], Kyung-Hun Lee[3], Jeong-Hyeon Kim[1],
Myung-Hyun Kim[1] and Jae-Myung Lee[*1]

[1]*Department of Naval Architecture & Ocean Engineering, Pusan National University,
Busan 609-735, South Korea*
[2]*Samsung Heavy Industries Co., Ltd., Geoje 656-710, South Korea*
[3]*Sungdong Shipbuilding & Marine Engineering Co., Ltd., Tongyeong 650-827, South Korea*

Abstract.   In general, cylindrically curved plates are used in ships and offshore structures such as wind towers, spa structures, fore and aft side shell plating, and bilge circle parts in merchant vessels. In a number of studies, it has been shown that curvature increases the buckling strength of a plate under compressive loading, and the ultimate load-carrying capacity is also expected to increase. In the present paper, a series of elastic and elastoplastic large deflection analyses were performed using the commercial finite element analysis program (MSC.NASTRAN/PATRAN) in order to clarify and examine the fundamental buckling and collapse behaviors of curved plates subjected to combined axial compression and lateral pressure. On the basis of the numerical results, the effects of curvature, the magnitude of the initial deflection, the slenderness ratio, and the aspect ratio on the characteristics of the buckling and collapse behavior of the curved plates are discussed. On the basis of the calculated results, the design formula was developed to predict the buckling and ultimate strengths of curved plates subjected to combined loads in an analytical manner. The buckling strength behaviors were simulated by performing elastic large deflection analyses. The newly developed formulations were applied in order to perform verification analyses for the curved plates by comparing the numerical results, and then, the usefulness of the proposed method was demonstrated.

1. Introduction

For several decades, finite element method has been dominantly used to analyze various structural engineering problems. Despite of the long history and the success in engineering fields, there have been unsolved issues in finite element method and continuous challenges are still desirable. Structural finite elements (shells, plates, and beams) have been derived from basic continuum mechanics and standard isoparametric procedures. However, the displacement-based finite elements are too stiff in bending-dominated situations when the thickness is small, regardless

---

*Corresponding author, Professor, E-mail: jaemlee@pusan.ac.kr

of the displacement interpolation order. The phenomenon is called as locking and numerous.

A cylindrically curved plate is the main component of ships and offshore structures. The curved plates dare normally used to assemble deck plating with a camber, fore and aft side shell plating, wind towers, and bilge circle parts in merchant vessels. These curved plates can undergo axial compressive loading from both hull girder bending and hydrostatic pressure by seawater. Nowadays, classification society standards such as LR, DNV, NK, and BV provide a guideline for estimating the buckling strength of a ship's curved plate. However, these classification society rules are unable to sufficiently solve the real problem. For example, the effect of curvature and the characteristic of the curved plate (i.e., slenderness ratio, aspect ratio, and initial deflection) are not exactly reflected. Furthermore, the design value that was suggested by the classification rules was different from the finite element analysis (FEA) result. Simulations carried out using cylinder models have shown that curvature causes an increase in the buckling strength of a curved plate undergoing combined loads (axial compression and lateral pressure), and this curvature is also expected to increase the ultimate strength (Karman *et al.* 1940, Karman and Tsien 1941).

In the present study, in order to clarify and examine the fundamental buckling behavior of a cylindrically curved plate under axial compressive loads, a series of elastoplastic large deflection analyses were carried out together with comparisons of the collapse behaviors of curved plates that had various flank angles, including nonlinear factors. On the basis of the calculated results, the effects of curvature (R), initial deflection (w), slenderness ratio (β), and aspect ratio (a/b) on the characteristics of the buckling and ultimate strength behaviors of the cylindrically curved plates and circular cylinders under axial compression are discussed, but the effect of residual stress from welding work is not considered. On the basis of results of a series of nonlinear finite element calculations for all edges of a plate set to a simply supported condition, the design formulae were derived as empirical formulae in order to predict the critical buckling strength and ultimate strength of curved plates. The predicted results showed good accuracy as compared to the results of the FEA.

1.1 Literature survey

In this section, a brief review of previous research related to the buckling and ultimate strength behaviors of cylindrically curved plates and stiffened plates is given.

Maeno *et al.* (2003, 2004) performed a series of elastoplastic large deflection analyses to investigate the buckling and plastic collapse behaviors of ship bilge strakes, which are typical in tanker and bulk carriers. These bilge strakes are unstiffened, curved, thick plates that are subjected to axial compression. Yumura *et al.* (2005) investigated the buckling and plastic collapse behaviors of cylindrically curved plates under axial compression. Park *et al.* (2005) performed nonlinear finite element method (FEM) analyses on actual stiffened curved plates of a container ship, varying the curvature and spacing of the stiffeners. Kwen *et al.* (2004) performed nonlinear FEM analyses for unstiffened curved plates, varying the aspect ratio, slenderness ratio, and curvature under various loading conditions such as longitudinal thrust, transverse thrust, and shear load. Cho *et al.* (2007) performed ultimate strength tests and nonlinear finite element analyses under axial compression on six curved, stiffened plates. An analytical approach using large deflection theory was proposed by Levy (1943) for simulating the elastic behavior of an initially curved sheet. Buermann *et al.* (2006) presented a fast, semi-analytical model for the post-buckling analysis of stiffened cylindrical panels. Kundu *et al.* (2007) investigated the geometrically nonlinear post-buckling analysis of laminated composite doubly curved shells by FEM. By
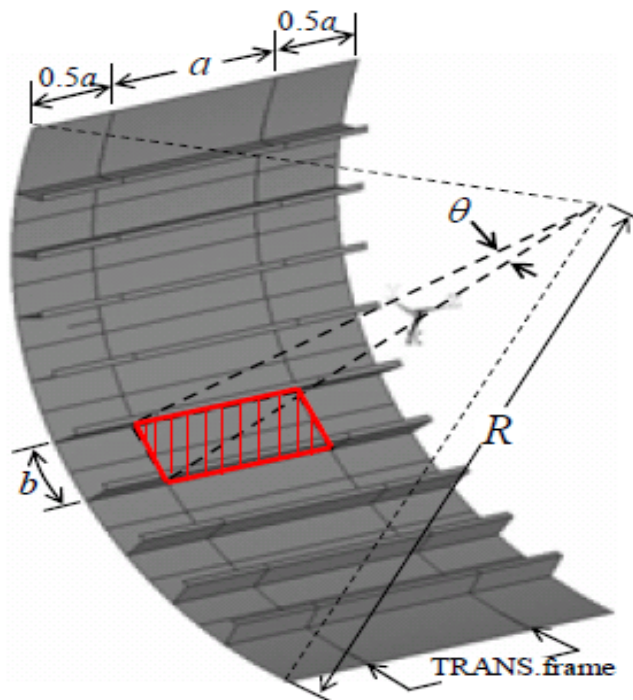
Fig. 1 Schematic of a cylindrically curved plate

applying the arc length method, both the snap-through and snap-back post-buckling behaviors were well captured. Park *et al*. (2008, 2009) performed nonlinear FEM analyses for unstiffened curved plates, varying the aspect ratio, slenderness ratio, and curvature under combined loading conditions, and developed an analytical method as well.

However, further studies are needed for facilitating more rational guidelines for the buckling and ultimate strength engineering concepts of curved plates. Curvature is the most important parameter dominating the buckling and plastic collapse behaviors of a cylindrically curved plate subjected to compressive loading. In general, curved plates in the bilge strakes of tankers and bulk carriers are so thick that plastic buckling occurs rather than elastic buckling. However, fundamentally, it is very important to clarify the buckling and collapse behaviors, particularly those under axial compression, by considering the ultimate hull-girder bending strength. It is well known that a thin flat plate undergoes secondary buckling after initial buckling. Similar behavior may take place in curved plates, so information on the elastic buckling behavior may be useful when the buckling behavior of curved plates with reduced thicknesses due to corrosion is considered. The buckling and plastic collapse behaviors of cylindrically curved plates as compared to flat plates should also be clarified. Studies comparing the buckling and plastic collapse behaviors and ultimate strength of curved plates to those of flat plates are lacking.

Therefore, in the present study, the buckling and collapse characteristics of a curved plate were analyzed according to various flank angles, and a new formula for estimating the ultimate and buckling strengths was developed in order to clarify the characteristics of a curved plate under axial compression. The validity of the newly developed formula was confirmed through comparisons with the finite element solutions.

Table 1 Material properties for the curved plate

Material	Elastic Modulus (GPa)	Poisson ratio	Yield Stress (MPa)	Aspect Ratio
AH32	206	0.3	315	2.2 3.7

2. Finite element analysis and numerical method

2.1 Analysis target modeling and scenario

The model for the finite element (FE) analysis was a simple curved plate without any stiffeners under various states of loading conditions such as longitudinal compression, transverse compression, and lateral pressure, and Fig. 1 shows the target curved plate. The cylindrically curved plate had dimensions of length a, width b, thickness t, and flank angle θ, and the length of the circular arc b was kept constant at 1000 mm throughout the study. The width b and flank angle θ are related by the formula $b = \theta R$, where R is the radius of curvature. Therefore, θ is the most important parameter for determining the buckling strength of the curved plate in these models. Four values including 5°, 10°, 20°, and 30° were used for the flank angle parameter (θ). On the basis of these model concepts, a series of eigenvalue buckling finite element analyses were carried out in order to evaluate the buckling strength and examine the significant buckling mode.

The 1/2 + 1/2 bay model is very effective for investigating a buckling pattern in a continuous plate, and it should be adopted to simulate the clamped mode as well as the simply supported mode, the one bay model was adopted. In the case of the 1/2 + 1/2 bay model, buckling and collapse behavior is changed depending on the dimensions of the stiffeners (longitudinal and transverse direction); hence, it is difficult to estimate a buckling strength and mode variation for isolated curved plate. In addition, the simply supported condition was adopted even though the clamped boundary condition should be considered when lateral pressure load is applied. In terms of structural design, when evaluating the buckling and ultimate strength for a curved plate, adopting a simply supported condition gives more conservative results compared to the clamped condition. Moreover, for the safe design of ships and offshore structures, this design approach of using the simply supported condition provides a proper safety factor. As a result, from the aspect of structural design, one bay model and simply supported condition was adopted in this research.

The material properties for the curved plate listed in Table 1. The analysis models incorporated an idealized elastic-perfectly plastic stress-strain curve, and the strain hardening rate was set to zero. The isotropic hardening law was assumed by employing the von Mises yield criterion. High tensile steel (AH32) was employed as the material of the curved plate. The elastic modulus (E) was 206 GPa, and the yield stress was 315 MPa.

The analysis scenario is summarized in Table 2. As mentioned before, the linear/nonlinear buckling analysis was carried out on a curved plate that had various flank angles (θ) and plate thicknesses (t) as the main parameters. The analysis was conducted with curved plate flank angles of 5°, 10°, 20°, and 30°, and additional flank angles such as 2° and 3° were added to the comparison trend according to the flank angle. Four types of loading conditions were applied to the curved plate. As a single load, longitudinal compression and transverse compression were considered. Moreover, as a combination of loads, biaxial compression, longitudinal compression and lateral pressure or transverse compression and lateral pressure that acted at the same time were considered.

Table 2 Analysis scenarios of the curved plate

Flank angle (°)	Plate thickness (mm)	Loading condition
0	10	Longitudinal compression
2	12	Transverse compression
3	14	Biaxial compression
5	16	Longitudinal compression and lateral pressure
10	20	
20	24	
30	30	Transverse compression and lateral pressure
	35	
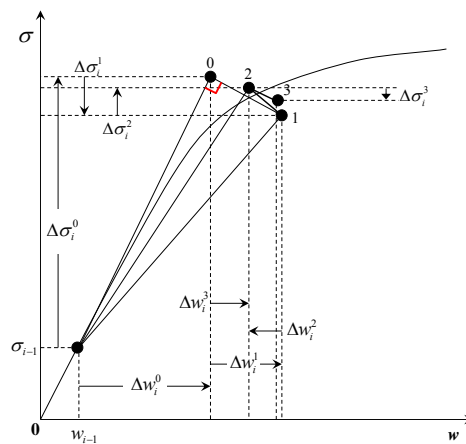
Fig. 2 Schematic of the arc-length method

2.2 Numerical method

In this study, the arc-length method was selected as the numerical method for predicting nonlinear buckling behavior. The conventional Newton-Raphson method fails to predict buckling behavior because of the singularity of the stiffness matrix and a diverging solution. However, the arc-length method is suitable for obtaining a nonlinear static solution of an unstable solution by tracking complex buckling behaviors such as secondary buckling, snapback, or snap through for thinner plates. For problems with sharp turns in the load-displacement curve or path dependent materials, it is necessary to limit the arc-length radius (arc-length load step size) using the initial arc-length radius. During the solution, the arc-length method will vary the arc-length radius at each arc-length substep according to the degree of nonlinearities that are involved. The arc length method was obtained using the principle of virtual work that was applied in incremental form. The theory of virtual work is shown by Eq. (1)

$$\delta \Delta W_e = \delta \Delta W_i \tag{1}$$

where ΔW_e is the external work and ΔW_i is the internal work. Therefore, virtual work can be rewritten by Eq. (2)

$$[K]\{\Delta W\} = \Delta \sigma \{R\} + \{Q\} \tag{2}$$

where [K] is stiffness matrix, $\{\Delta W\}$ is nodal displacement increment, $\Delta\sigma$ is load scale parameter, $\{R\}$ is applied nodal force vector, and $\{Q\}$ is unbalance force to be converged. By applying Eq. (2), the arc-length methods can be represented by Eqs. (3)-(7). At step $i-1$, the incremental form can be represented by Eq. (3) as follows

$$[K(W_{i-1})]\{\Delta W_i^0\} = \{Q_{i-1}\} + \Delta\sigma_i^0\{R(W_{i-1})\} \tag{3}$$

where R is the reference arc-length radius, ΔW is the increment of the deflection component, and is the average stress at step i. The arc length must satisfy the following relation:

$$\|\Delta W\|^2 + \left(\Delta\sigma_i^0\right)^2 = r_i^2 \tag{4}$$

where r_i is the arc length at step i and the first increment of the arc length at step i $\{\Delta W_i^0, \Delta\sigma_i^0\}$ as well; the two parameters are also in the same direction. Therefore, they can be linearized as follows

$$\left\{\sum_{m=0}^{l}\Delta W_{i-1}^m\right\}^T \{\Delta W_i^0\} + \sum_{m=0}^{l}\Delta\sigma_{i-1}^m\Delta\sigma_i^0 = r_i^2 \tag{5}$$

Since Eqs. (3) and (5) can be solved as a linear system, $\{\Delta W_i^0\}$ and $\{\Delta\sigma_i^0\}$ can be calculated as shown in Eq. (6)

$$\begin{bmatrix} K(W_{i-1}) & -R(W_{i-1}) \\ \sum_{m=0}^{l}\Delta W_{i-1}^{m\,T} & \sum_{m=0}^{l}\Delta\sigma_{i-1}^m \end{bmatrix}\begin{Bmatrix} \Delta W_i^0 \\ \Delta\sigma_i^0 \end{Bmatrix} = \begin{Bmatrix} Q_{i-1} \\ r_i^2 \end{Bmatrix} \tag{6}$$

During the repeat and convergence calculation of the *n*-steps, the stiffness matrix equation can be represented as follows

$$\left[K(W_{i-1} + \sum_{m=0}^{n}\Delta W_i^m)\right]\{\Delta W_i^n\} - \Delta\sigma_i^n\left\{R(W_{i-1} + \sum_{m=0}^{n-1}\Delta W_i^m)\right\} = \{Q_i^{n-1}\} \tag{7}$$

where $\{Q_i^{n-1}\}$ represents the nonparallel force, as shown in Eq. (7). The arc-length r_i is needed to satisfy same length, and can be represented by Eq. (8)

$$\left\|\sum_{m=0}^{n-1}\Delta W_i^m + \Delta W_i^n\right\|^2 + \left(\sum_{m=0}^{n-1}\Delta\sigma_i^m + \Delta\sigma_i^n\right)^2 = r_i^2 \tag{8}$$

Eq. (8) can be linearized as shown in Eq. (9)

$$\left\{\sum_{m=0}^{n-1}\Delta W_i^m\right\}^T \{\Delta W_i^n\} + \sum_{m=0}^{n-1}\Delta\sigma_i^m\Delta\sigma_i^n = 0 \tag{9}$$

As the system of linearization can make Eq. (4) and (6), ΔW_i^n and $\Delta\sigma_i^n$ can be calculated as shown in Eq. (10)

$$\begin{bmatrix} K(W_{i-1} + \sum_{m=0}^{n-1} \Delta W_i^m) & -R(W_{i-1} + \sum_{m=0}^{n-1} \Delta W_i^m) \\ \sum_{m=0}^{n-1} \Delta W_{i-1}^{m\,T} & \sum_{m=0}^{n-1} \Delta \sigma_{i-1}^m \end{bmatrix} \begin{Bmatrix} \Delta W_i^n \\ \Delta \sigma_i^n \end{Bmatrix} = \begin{Bmatrix} Q_i^{n-1} \\ 0 \end{Bmatrix} \tag{10}$$

In this calculation, Eq. (10) is repeated until the nonparallel force $\{Q_i\}$ is equal to zero before the calculation is terminated.

2.3 Initial deflection

Initial imperfections, such as residual stress or initial deflection, exist in the manufacturing and assembly processes by thermomechanical processes such as cutting and welding. The initial deflection wave is generally represented as Eq. (11). Eq. (11) was derived by idealizing plate to beam and assuming boundary condition to simply support (Smith 1988).

$$w_o = \sum_{m=1}^{\infty} \sum_{n=1}^{\infty} A_{omn} Sin \frac{m\pi x}{a} Sin \frac{n\pi y}{b} \tag{11}$$

Fig. 3(a) shows the initial deflection shape of the eigenvalue model through an elastic buckling analysis under longitudinal compressive load. Fig. 3(b) shows an example of the initial deflection shape due to welding. This deflection shape has an asymmetric in the longitudinal direction. Although the initial deflection modes are different, the first mode obtained by the eigenvalue analysis was applied as the initial deflection shape. Because the collapse modes were shown to be equal, there is little impact on the behavior of the buckling and ultimate strengths according to the initial deflection shape. Therefore, in this study, the curved plate was assumed to go through the buckling mode from initial deflections that occurred by welding. The maximum initial deflection is determined by Eq. (12).

$$w_0 = 0.05\beta^2 t \tag{12}$$

where t is the thickness of the plate and β represents the slenderness ratio of plate, which is calculated using Eq. (13)

$$\beta = \frac{b}{t} \sqrt{\frac{\sigma_Y}{E}} \tag{13}$$

where b is the breadth of the plate, σ_Y is the yield strength of high tensile steel, and E represents the elastic modulus. The Smith equation was used as in the format of Eq. (12), and the factor was controlled to 0.05 in order to reflect the actual amount of initial deflection. This was done because the distinction of the initial deflection proposed by gave a conservative result when compared with actual measured data. Therefore, the factor of Eq. (12) was applied in accordance with the actual measurement data (Ueda and Yao 1987). The effect of the initial deflection is considered in this study, but the effect of residual stress was not.

2.4 Mesh convergence study

As shown in Fig. 4, a mesh convergence study was carried out for flat plates under longitudinal compression using three kinds of FEA tools such as MSC.NASTRAN, ANSYS, and ABAQUS.

(a)	(b)
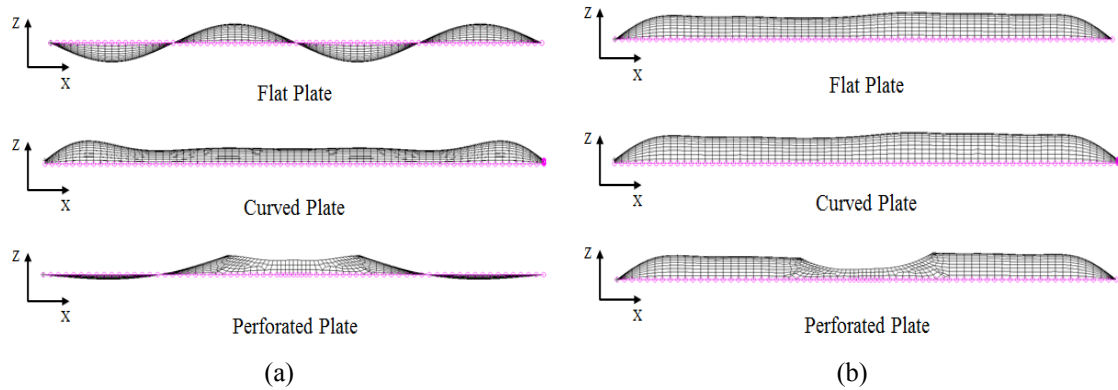
Fig. 3 Initial deflection shapes produced by (a) eigenvalue analysis and (b) welding
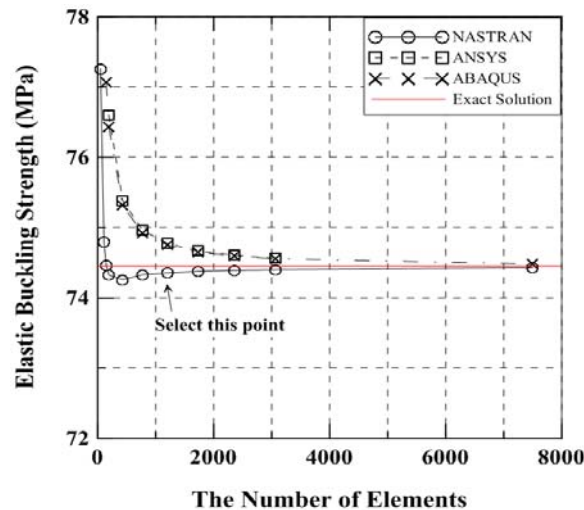
Fig. 4 Mesh convergence study of the flat plate

An eigen buckling analysis of elastic buckling strength was the same for each, but nonlinear analysis showed a different result in each case. The number of meshes was determined by comparing the exact solution with the result of the buckling analysis when the value of the buckling strength began to converge to the reference value. When the aspect ratio was 3.0, a reasonable mesh number was 20×60 for the flat plate to reduce the time loss. When the mesh number was 20×60, the buckling strength did not differ from analyses of plates that had higher mesh numbers. Therefore, the mesh of the curved plate was set to 20×60 in this study. At this time, the error between the FEA and the exact solution is 1% or less. Moreover, this mesh size is widely used among many designers, making it a reasonable selection.

3. Finite element analysis result

3.1 Eigen buckling result

In order to evaluate the buckling strength and examine the significant buckling mode, a series of eigenvalue buckling analyses of the curved plate were carried out. The eigenvalue result of the buckling analysis was used to produce a shape of the initial deflection that was reflected to the nonlinear analysis. Fig. 5 shows the typical buckling modes for various flank angles and slenderness ratios. When the flank angle was zero, as is the case for a flat thinner plate, the plate's buckling occurred in four half-waves in the longitudinal direction. However, as the flank angle increased to 5°, the buckling mode changed so that the deflection flattened out towards the loading direction, and the deflection locally grew at the loading edges, as shown in Fig. 5(a) with a flank angle of 5° at 10 mm thickness. When the flank angle was greater than these values, buckling took place in an irregular mode, as indicated in Fig. 5(a). For larger thicknesses of the plate, four or five half-wave modes appeared in the loading direction, as shown in Fig. 5(a) with a flank angle of 5° and thicknesses of 24 mm and 35 mm. In general, the buckling mode of the plate under transverse compressive loading took place in one half-wave in the transverse direction; however, the plate with curvature appeared in the circumferential direction at the local parts, as shown in Fig. 5(b) with a flank angle of 30° and thickness of 20 mm. This was considered as a part of the shell buckling of a cylinder wall and is called the diamond buckling mode.

The elastic buckling modes of a curved plate under longitudinal compression with various flank angles are shown in Fig. 6. The solid red lines represent the compressive load, and the solid blue

Flat plate [10mm]	Flat plate [10mm]
Curved plate [5 degree, 10 mm]	Curved plate [5 degree, 10 mm]
Curved plate [5 degree, 24 mm]	Curved plate [5 degree, 35 mm]
Curved plate [5 degree, 35 mm]	Curved plate [30 degree, 20 mm]
(a)	(b)
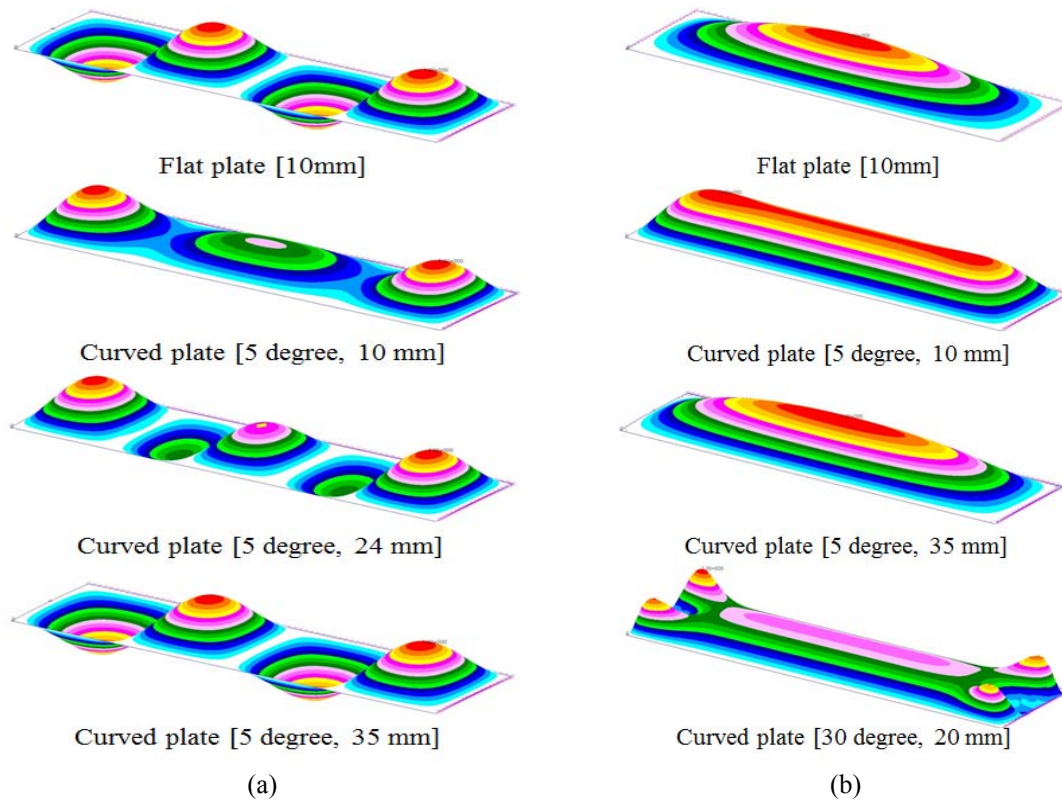
Fig. 5 Typical buckling modes obtained by elastic eigenvalue analyses (a) longitudinal compression and (b) transverse compression
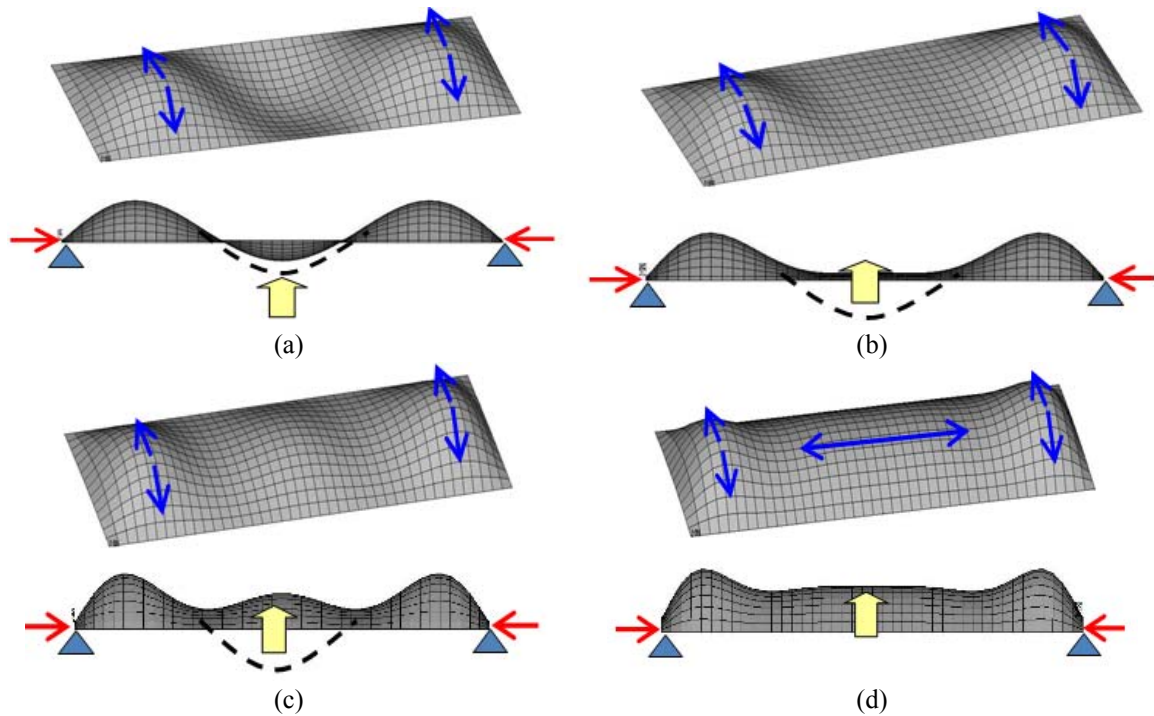
Fig. 6 Elastic buckling mode with varying flank angles (a) 2°, (b) 3°, (c) 5°, and (d) 10° under longitudinal compression

lines represent tension. When the longitudinal compressive loading is acting on the curved plate, the tensional membrane force occurs throughout the plate, affecting the buckling strength. This can be observed in Fig. 6(a)-(d). As indicated in Fig. 6(a), when the flank angle was less than or equal to 2°, the buckling took place with three longitudinal half-waves as in the case of a rectangular flat plate. As the flank angle increases, as shown in Fig. 6(b), the middle part of the half-wave upheaves, abruptly changing the buckling mode from three half-waves to two half-waves. When the flank angle is further increased to 10°, as shown in Fig. 6(d), the longitudinal half-waves of the flat plate are changed from three half-waves to a single longitudinal half-wave with additional swelled components of deflection near the transverse edges, caused by the tensional membrane forces. The tensional forces occurring vertically in both ends spread to the middle of the curved plate in the longitudinal direction. The longitudinal tensional membrane forces occurring in the middle of the curved plate thus restrain the outward deflection. In other words, the buckling strength is higher than that of the flat plate owing to the membrane force effect produced by the deflection. This is observed in Fig. 6(b) and Fig. 6(d).

3.2 Benchmark study

A comparative analysis was performed between the classification society rules and a finite element method (FEM) eigenvalue buckling analysis for the critical buckling strength of a curved plate. The comparative results of σ_{cr}/σ_y for each case are shown in Fig. 7 with the formulae for σ_{cr} described below. The elastic buckling strength in the classification society rules has been derived
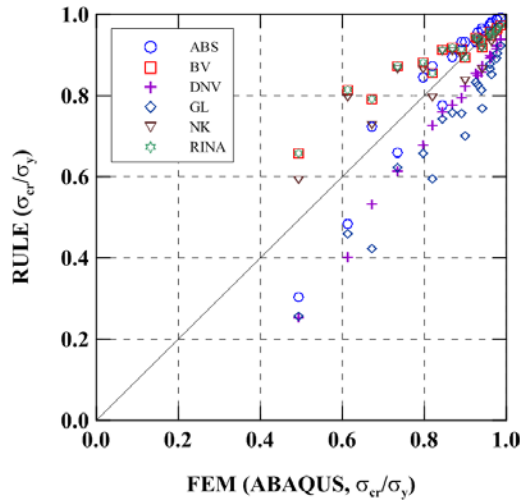
Fig. 7 Verification of the results of buckling strength for the curved plate under axial compression

using Euler's buckling formula with an empirical plasticity correction applied when the elastic buckling strength is greater than 50% of the yield strength. The eigenvalue buckling results were obtained by finite element analysis (FEA) using the ABAQUS software suite. The Johnson-Ostenfeld correction formula was used for plasticity correction of both the classification society rules as well as the eigenvalue buckling analysis to allow for direct comparison. The critical buckling strength based on the Johnson-Ostenfeld formula is given as follows

$$\sigma_{cr} = \begin{cases} \sigma_E & for \, \sigma_E \le 0.5\sigma_F \\ \sigma_F[1-\sigma_F/(4\sigma_E)] & for \, \sigma_E > 0.5\sigma_F \end{cases} \tag{14}$$

In the formulae above, σ_{cr} refers to the critical (elastic-plastic) buckling stress; σ_E, to the elastic buckling stress; and σ_F, to the reference yield stress. When performing the eigenvalue buckling analysis using the ABAQUS suite, the "Buckle" step was performed in the software, and subsequent buckling analyses were performed to evaluate the eigenmode (only mode 1 is considered in this study) and eigenvalue of the structure; the Lanczos solver was used as it provides the most accurate values in elastic buckling analysis. In this step, additional incremental analysis is unnecessary because the increment size is calculated automatically by the ABAQUS program.

As shown in Fig. 7, a comparison of the two results was made in which the critical buckling strengths from both the FEM and class rule calculations were relatively similar in the case of the thicker plate. In the case of the thinner plate, however, the FEM results of the critical buckling strength showed significant differences owing to the curvature reduction factor, which is normally adopted in the classification society's equations. In other words, the curvature reduction factor of the classification society's equations cannot reflect the buckling phenomenon exactly.

Therefore, in this study, the curvature reduction factor should be found by nonlinear buckling analysis and a design formula that gives a more accurate result than class's rule, and should be developed in order to easily estimate the critical buckling strength by the reflecting curvature factor.
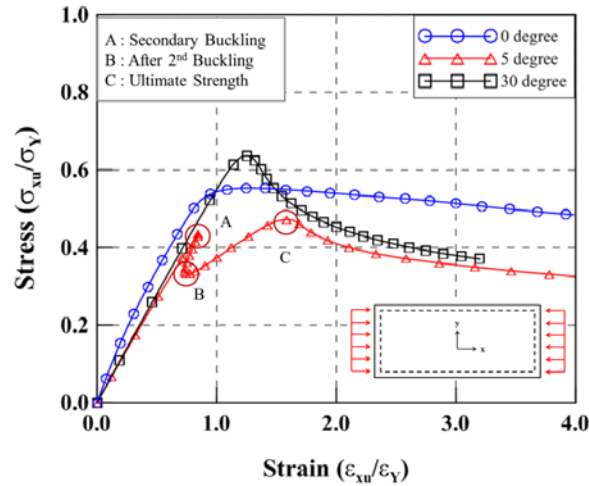
Fig. 8 Relationships between average stress and average strain of the plate with or without curvature under longitudinal compression ($t = 10$)

3.3 Progressive collapse behavior

A series of elasto-plastic large deflection analyses were performed to clarify the fundamentals in progressive collapse behavior including occurrence of buckling and yielding of cylindrically curved plates under axial compression. The thickness of the plate was varied from 10 mm to 35 mm. For each case, the average stress-average strain relationships, including the case of a flat plate (0°), were calculated and the representative analysis result at a thickness of 10 mm was summarized in Figs. 8 and 10.

First, the progressive collapse behavior of a thin plate subjected to compressive load is explained in Fig. 8 when the flank angle was 5°, the secondary buckling took place at point A, as shown in Fig. 8. Then, the load-carrying capacity rapidly decreased because of the occurrence of secondary buckling accompanied by the snap-back unloading phenomenon. At that time, the buckling mode abruptly changed from one half-wave to three half-waves in the loading direction. The final collapse mode further changed from three half-waves to five half-waves against the increase in compressive loading, as shown in Fig. 9.

This change in collapse mode occurred because of the secondary buckling after the primary buckling. It is known that the secondary buckling strength of a simply supported plate is very high, but for the aspect ratio at which the buckling mode terminates, the secondary buckling strength is relatively low. Such high-order buckling after the primary buckling takes place because of the change in the in-plane stress distribution due to a large deflection (Paik and Thyamballi 2003, Paik *et al.* 2003). This is because the snap-back phenomenon occurs under particular conditions such as a certain aspect ratio, specific slenderness ratio, thin plate, and low flank angle (Kwon and Hancock 1991, Madenci and Barut 1994, Byklum and Amdahl 2002). This snap-back behavior can be captured using arc-length control with incremental force by compressive load. Specifically, the ultimate strength of the thin plate ($t = 10$ mm) was estimated to be lower than that of the flat plate owing to the occurrence of secondary buckling. In the case of the ultimate strength of the curved plate with a small flank angle, the secondary buckling behavior should be carefully considered. With a further increase in the curvature, the buckling and ultimate strengths gradually increased;

(a)

(b)

(c)
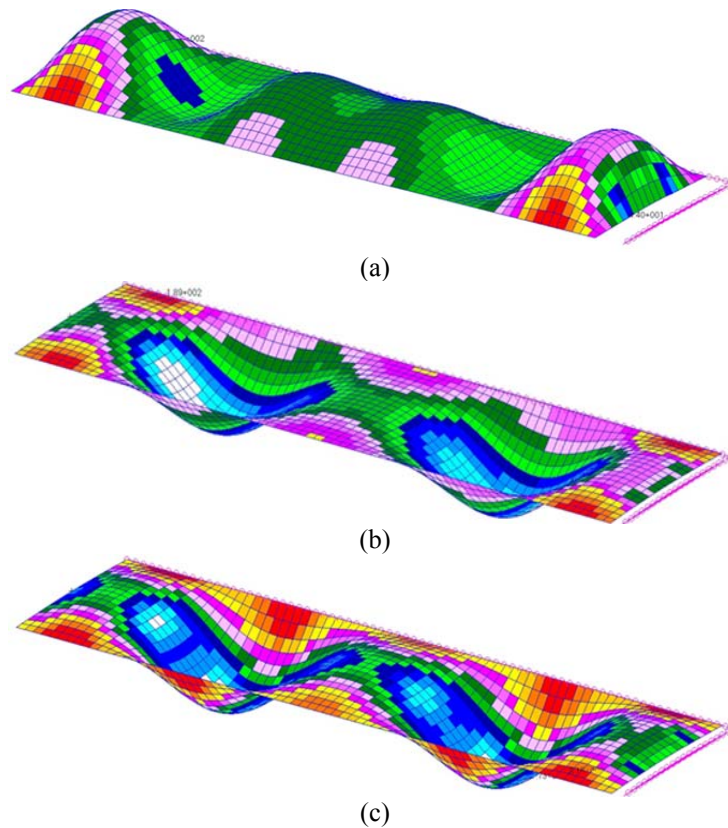
Fig. 9 Change in collapse modes of the curved plate ($t = 10$) with a flank angle of 5° (a) one half wave mode ($\varepsilon_{xu}/\varepsilon_Y$=0.8), (b) three half wave mode ($\varepsilon_{xu}/\varepsilon_Y$=0.9), and (c) five half wave mode ($\varepsilon_{xu}/\varepsilon_Y$=1.6)

thus, the buckling and yielding started to take place, and the ultimate strength was attained. Fig. 10 shows the average stress and average strain curves under transverse compression with varying curvature at the same thickness ($t = 10$ mm). When transverse compression was applied to the curved plate, buckling and yielding started at the short edges and the ultimate strength was attained. In the post-ultimate strength, yielding was restricted only near the ends where buckling deflection was produced. This implies that the middle of the plate remained in the elastic range. Thus, on the basis of the results shown in Fig. 10, the buckling and ultimate strengths decreased with an increase in the curvature. However, this characteristic was different for loading in the longitudinal direction.

3.4 Influence of slenderness ratio and initial deflection

A series of FEM analyses were performed by changing the slenderness ratio of the curved plate from 1.18 to 4.14. These slenderness ratios were obtained by changing the thickness of the plate between 10 mm and 35 mm and keeping the breadth and the length of the plate constant at 1,000 mm and 3,700 mm, respectively. The flank angle was taken as 5°, 10°, 20°, and 30°. These results were compared with the Faulkner equation and flat plate. The calculated ultimate strength was plotted against the slenderness ratio, as shown in Fig. 11.
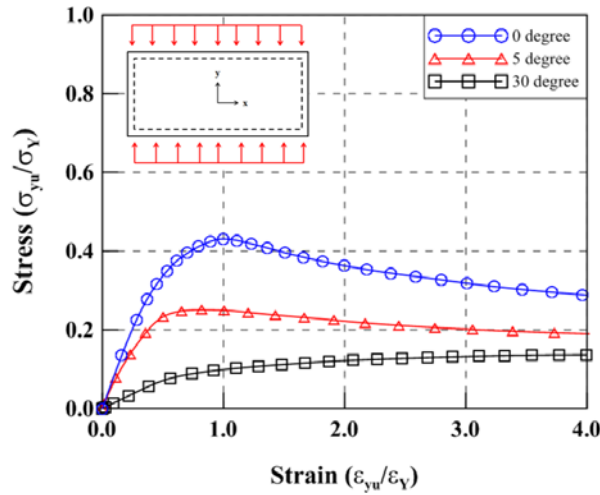
Fig. 10 Relationships between average stress and average strain of the plate with or without curvature under transverse compression ($t = 10$)

(a)　　　　　　　　　　　(b)
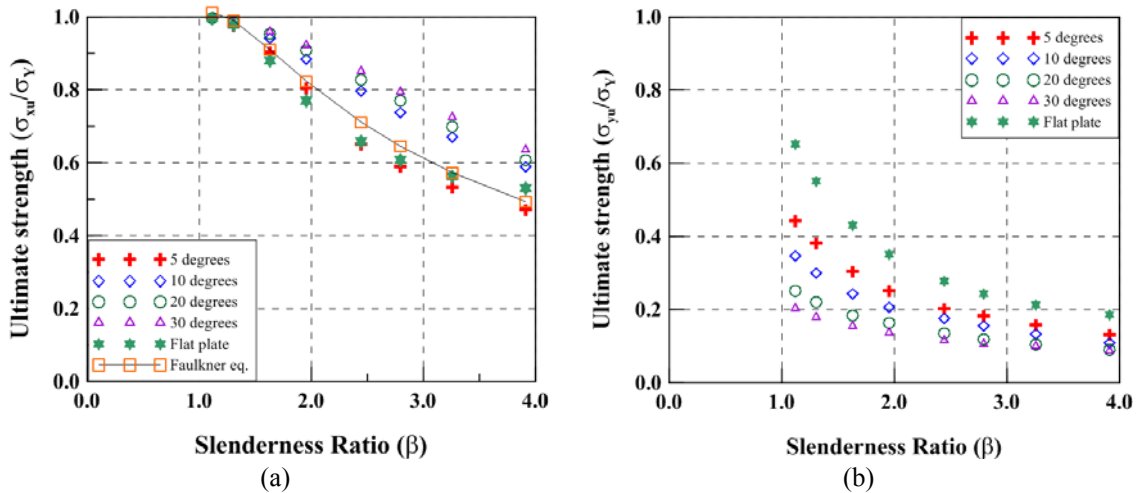
Fig. 11 Relationships between ultimate strength and slenderness ratio with various curvatures under (a) longitudinal compression and (b) transverse compression

It can be seen that the ultimate strength of the curved plate with a flank angle of 5° was lower than that of a flat plate under the longitudinal direction caused by the secondary buckling. In addition, the ultimate strength did not increase in the case of a curved plate for a flank angle of 5° because of the initial deflection effect for the curved surface at a low flank angle. In addition, the ultimate strength of the curved plate at 5° was underestimated because the curved surface at this low flank angle could act as an deflection that added to the initial deflection. However, in the case of the curved plate with a high flank angle, the ultimate buckling strength was higher than that of the flat plate owing to the membrane effect in the circumferential direction. This phenomenon is explained in detail in section 3.3. Fig. 11(b) shows the relationship between the average stress and slenderness ratio with various curvatures under transverse compression. The differences in
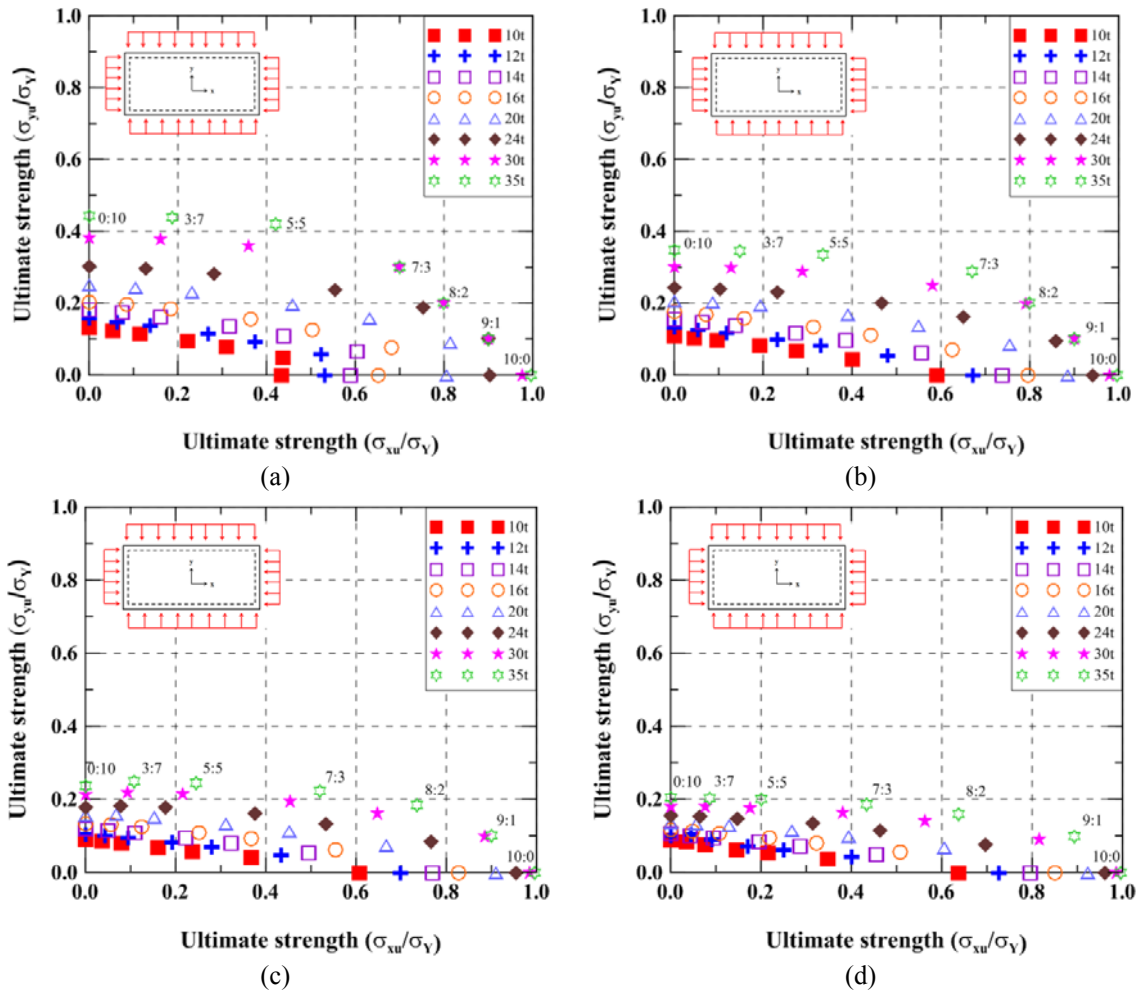
Fig. 12 Relationships between ultimate strength of longitudinal compression and transverse compression while varying the curvature under biaxial compression (a) 5°, (b) 10°, (c) 20°, and (d) 30°

ultimate strengths with different thicknesses were small over a flank angle of 20°.

Fig. 12 shows the ultimate strength interaction relationship of a curved plate under combined biaxial compressive loads as a function of the plate thickness. The loading ratios (longitudinal compressive loading to transverse compressive loading) were 9:1, 8:2, 7:3, 5:5, and 3:7. With the increase in the plate thickness, the load-carrying capacity also increased for various combinations of stress components.

Furthermore, the buckling analysis was conducted to evaluate this trend by comparing between the simply supported condition and the clamped condition. The current practical design criteria in classification society rules for the buckling and ultimate strengths of a cylindrically curved plate are based on the assumption that all edges are simply supported. In actual ship plating, the idealized edge conditions (e.g., simply supported or clamped condition) may never occur because of finite rotational restraints. To investigate the ultimate strength of a cylindrically curved plate under different boundary conditions, a series of calculations were performed considering two
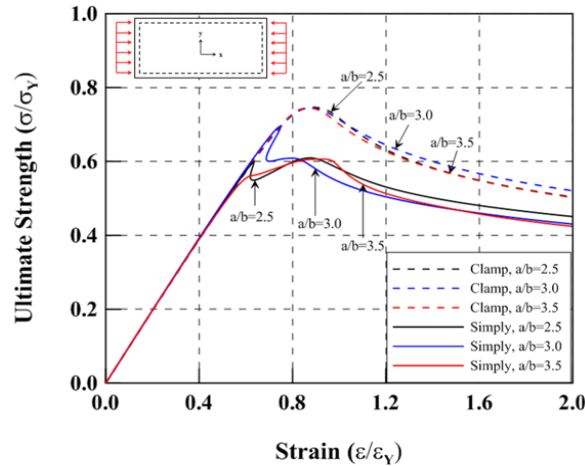
Fig. 13 Comparisons of the average stress and average strain of the curved plate with two types of boundary conditions under axial compression (t = 15 mm, θ = 5°)

kinds of boundary conditions (all edges simply supported condition and all edges clamped condition).

Fig. 13 shows the relationships between average stress and average strain of a curved plate with a flank angle of 5° considering two kinds of boundary conditions under longitudinal compression. The ultimate strength for the clamped condition was generally higher than that for the simply supported condition.

In some cases, however, particularly for the case of thin plate (e.g., t = 8 mm, θ = 30°), the ultimate strength of the curved plate in the clamped condition was lower than that of the simply supported condition. In general, the secondary buckling strength decreases as the constraint against rotation along the edges increases. This is why secondary buckling occurs when edges are clamped and not when edges are simply supported. As a result, the ultimate strength in the simply supported condition was lower than the ultimate strength in the clamped condition. On the basis of the above discussions, it is considered reasonable to apply the FEA results to the development of empirical formulae because the simply supported condition result contained the proper size of the safety factor.

4. Formula development

4.1 Buckling strength formulation

This formulation was developed to easily estimate buckling strength. The distribution of buckling strengths over various slenderness ratios remained similar for flank angles over 10°. However, in case of small flank angles (5° or less) the tendency was different mainly owing to the change in curvature. In the present formulation, the conventional Euler buckling format was used and the correction factor was re-adopted as C_B, C_R and C_J by Eqs. (15)-(22). This formulation followed the calculation of the plasticity correction by Johnson-Ostenfeld. In general, the Euler buckling stress (σ_E) was greater than half the yield stress (σ_Y), with the critical buckling stress

given by $\sigma_{J-O}=[1-(\sigma_Y/4\sigma_E)]\times\sigma_Y$, assuming that the proportional limit was $0.5\sigma_Y$. From these results, it was found that the developed formula could predict a buckling strength that was generally in good agreement with the FEM results.

$$\sigma_{E-LC} = k\frac{\pi^2 E}{12(1-v^2)}\left(\frac{t}{b}\right)^2 \times C_B \tag{15}$$

$$C_B = \sqrt{(1-v^2)}\times\theta\times\frac{\beta}{\sqrt{\sigma_Y/E}}\times C_R \tag{16}$$

$$C_R = 0.0323\left(\frac{R}{t}\right)^{-0.751}\times C_J \tag{17}$$

$$C_J = \begin{cases} 1.0 & \text{for } \beta<2.0 \\ 0.88 & \text{for } \beta\geq2.0 \end{cases} \text{ at } 0\leq\theta\leq10 \tag{18}$$

$$C_J = \begin{cases} 1.0 & \text{for } \beta<2.0 \\ 1.1 & \text{for } \beta\geq2.0 \end{cases} \text{ at } 10<\theta\leq30 \tag{19}$$

where σ_{E-LC} is the buckling strength of the curved plate under longitudinal compressive load. The coefficient of buckling strength (C_B) was assumed to be a function of curvature and slenderness ratios of the curved plate and the coefficient of reduction (C_R). The function of C_J represented the effect of curvature. The final coefficient (C_J) was set as a correction factor to represent the buckling mechanism.

$$\sigma_{E-TC} = k\frac{\pi^2 E}{12(1-v^2)}\left(\frac{t}{b}\right)^2 \times C_B \tag{20}$$

$$C_B = \sqrt{(1-v^2)}\times\theta\times\frac{\beta}{\sqrt{\sigma_Y/E}}\times C_R \tag{21}$$

$$C_R = 0.003\left(\frac{R}{t}\right)^{-1.514} \tag{22}$$

where σ_{E-TC} is the buckling strength of the curved plate under transverse compressive load.

4.2 Ultimate strength formulation

On the basis of the insights noted above, the ultimate strength of the cylindrically curved plate under axial compression may be empirically derived by curve fitting the FE results, and the new expression of Frankland's formula was used including the new factors. This method was considered reasonable to use because it was also adopted by the US Navy. This expression had the same general form as the Faulkner and Guedes Soares expressions, but the coefficients were different, leading to a more conservative prediction (Frankland 1940, Faulkner 1975, Guedes

Soares 1988). The accuracy of the present formula plotted against the slenderness ratio was checked by a comparison with FE solutions for a range of flank angles between 5° and 30°, as shown in Fig. 14 (red circle and blue triangle symbols). The correlation ratio and standard deviation of the curved plate subjected to longitudinal compression in the empirical formula as compared to the FEA were found to be 0.99 and 0.133, respectively. Moreover, the empirical formula of the curved plate under transverse compression had a correlation ratio of 0.99 and standard deviation of 0.08 when compared to the ultimate strength obtained by the FEA. The newly developed ultimate strength formula for a curved plate could give a reasonable estimation as compared to FEM results.

$$\frac{\sigma_{U\_LC}}{\sigma_Y} = \left(\frac{2.25}{\beta} - \frac{1.25}{\beta^2} \right) \times C_F \tag{23}$$

$$C_F = \frac{C_a}{\beta^2} + \frac{C_b}{\beta} + C_c \tag{24}$$

$$\left. \begin{aligned} C_a &= 3.434 \left(\frac{R}{t} \right)^2 - 1.989 \left(\frac{R}{t} \right) + 0.646 \\ C_b &= -4.138 \left(\frac{R}{t} \right)^2 + 1.934 \left(\frac{R}{t} \right) - 1.023 \\ C_c &= 1.001 \left(\frac{R}{t} \right)^2 - 0.181 \left(\frac{R}{t} \right) + 1.382 \end{aligned} \right\} \quad \text{for longitudinal compressive load} \tag{25}$$

$$\left. \begin{aligned} C_a &= 2.596 \left(\frac{R}{t} \right)^2 - 1.712 \left(\frac{R}{t} \right) + 0.415 \\ C_b &= -2.095 \left(\frac{R}{t} \right)^2 + 0.929 \left(\frac{R}{t} \right) - 0.136 \\ C_c &= 1.009 \left(\frac{R}{t} \right)^2 - 0.724 \left(\frac{R}{t} \right) + 0.322 \end{aligned} \right\} \quad \text{for transverse compressive load} \tag{26}$$

where the σ_{U_LC} is ultimate strength of the curved plate under longitudinal compressive load. The coefficient C_F was assumed as a function of the double slenderness ratio, and the correction factors (C_a, C_b and C_c) represented the effect of curvature with the change in the thickness of the plate.

$$\frac{\sigma_{U\_LCLP}}{\sigma_Y} = \left(\frac{2.25}{\beta} - \frac{1.25}{\beta^2} \right) \times C_F \times C_P \tag{27}$$

$$\left. \begin{aligned} C_a &= -0.068 \\ C_b &= 0.181 \\ C_c &= 0.883 \end{aligned} \right\} \quad \text{at } \theta \leq 10 \tag{28}$$
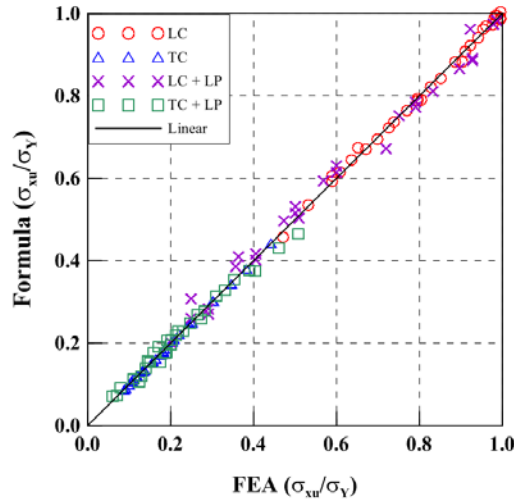
Fig. 14 Correlation of the empirical formula with ultimate strength obtained by the FEM of the curved plate under single and combined loads

$$
\left.
\begin{aligned}
C_a &= 3.434\left(\frac{b}{R}\right)^2 - 1.989\left(\frac{b}{R}\right) + 0.646 \\[2mm]
C_b &= -4.138\left(\frac{b}{R}\right)^2 + 1.934\left(\frac{b}{R}\right) - 1.023 \\[2mm]
C_c &= 1.001\left(\frac{b}{R}\right)^2 - 0.181\left(\frac{b}{R}\right) + 1.382
\end{aligned}
\right\} \quad \text{at } 10 < \theta \le 30 \tag{29}
$$

$$
C_P = -0.210\beta + 1.263 \tag{30}
$$

where the σ_{U_LCLP} is ultimate strength of the curved plate under combined longitudinal compressive load. The coefficient C_p was assumed as a function of the slenderness ratio, and the other factors (C_a, C_b and C_c) represented the effect of curvature with the change in the thickness of the plate.

$$
\frac{\sigma_{U\_TCLP}}{\sigma_Y} = \left(\frac{2.25}{\beta} - \frac{1.25}{\beta^2}\right) \times C_F \times C_P \tag{31}
$$

$$
\left.
\begin{aligned}
C_a &= 2.596\left(\frac{b}{R}\right)^2 - 1.712\left(\frac{b}{R}\right) + 0.415 \\[2mm]
C_b &= -2.096\left(\frac{b}{R}\right)^2 + 0.929\left(\frac{b}{R}\right) - 0.136 \\[2mm]
C_c &= 1.009\left(\frac{b}{R}\right)^2 - 0.724\left(\frac{b}{R}\right) + 0.322
\end{aligned}
\right\} \tag{32}
$$

$$C_P = -0.196\beta^2 + 0.893\beta + 0.314 \tag{33}$$

where the σ_{U_TCLP} is ultimate strength of the curved plate under combined transverse compressive load. As shown in Fig. 14 (purple X symbol), it was noted that the correlation ratio and standard deviation in the empirical formula of the curved plate subjected to combined longitudinal compression and lateral pressure when compared to the FEA were 0.99 and 0.27, respectively. The normalized ultimate strength as determined by the FEA was plotted against the normalized ultimate strength from the empirical formula of the curved plate under combined transverse compression and lateral pressure (green rectangle symbol). Both of these results also showed good agreement.

5. Conclusions

The objective of the present paper was to clarify and examine the fundamental buckling and plastic collapse behaviors and ultimate strength of a cylindrically curved plate under a variety of loading conditions (compression and combined compression and lateral pressure). On the basis of the calculated results, the effects of curvature, slenderness ratio, and loading effect on the buckling and ultimate strength were discussed. A simple formula was developed as an efficient method for predicting the critical buckling strength and ultimate strength. From this, we can draw the following conclusions:

• The curved plate under longitudinal compression had higher buckling and ultimate strengths than the flat plate with increasing curvatures because of the effect of curvature, except for the case in which the curvature is low.

• The buckling mode of a cylindrically curved plate under longitudinal compression took place with several half-waves in the loading direction when secondary buckling occurred. When secondary buckling did not occur, only the local regions near the loading edges collapsed.

• The buckling of the curved plate with relatively large flank angles took place in one half-wave mode in the loading direction with the local swelled shape near the loading edges. After the occurrence of primary buckling, secondary buckling took place and deflection changed to a mode with a larger number of half-waves. Furthermore, the in-plane rigidity decreased.

• The ultimate strength of the curved plate reduced significantly when secondary bucking occurred. At that time, the in-plane stress can be re-distributed with an abruptly occurring buckling mode change.

• The curved plate under transversal compression underestimated the buckling and ultimate strength with an increase in the curvature. This was mainly induced by the collapse pattern.

• A simple formula developed for a curved plate could give a reasonable estimate of buckling and ultimate strengths of the curved plate under a variety of loading conditions (longitudinal and transverse compressive loads, combined biaxial compression, and lateral pressure)

• Good correlations were observed with the ultimate strength and the buckling strength by applying the proposed empirical formula.

References

Buermann, P., Rolfes, R., Tessmer, J. and Schagerl, M. (2006), "A semi-analytical model for local post-buckling analysis of stringer and frame- stiffened cylindrical panels", *Thin Wall. Struct.*, **44**(1), 102-114.

Byklum, E. and Amdahl, J. (2002), "A simplified method for elastic large deflection analysis of plates and stiffened panels due to local buckling", *Thin Wall. Struct.*, **40**(11), 925-953.

Cho, S.R., Park, H.Z., Kim, H.S. and Seo, J.S. (2007), "Experimental and numerical investigations on the ultimate strength of curved stiffened plates", *Proceedings of the Tenth International Symposium on Practical Design of Ships and Other Floating Structures*, Houston, Texas, USA.

Faulkner, D. (1975), "A review of effective plating to be used in the analysis of stiffened plating in bending and compression", *J. Ship Res.*, **19**(1), 1-17.

Frankland, J.M. (1940), "The strength of ship plating under edge compression", US EMB Report 469.

Guedes Soares, C. (1988), "Design equation for the compressive strength of unstiffened plate elements with initial imperfections", *J. Constr. Steel. Res.*, **9**(4), 287-310.

Karman, T. and Tsien, H.S. (1941), "The buckling of thin cylindrical shells under axial compression", *J. Space. Rocket.*, **40**(6), 898-907.

Karman, T., Dunn, L.G. and Tsien, H.S. (1940). "The influence of curvature on the buckling characteristics of structures", *J. Aeronaut. Sci.*, **7**(7), 276-289.

Kundu, C.K. and Sinha, P.K. (2007), "Post buckling analysis of laminated composite shells", *Compos. Struct.*, **78**(3), 316-324.

Kwen, Y.W., Park, Y.I., Paik, J.K. and Lee, J.M. (2004), "Buckling and ultimate strength characteristics for ship curved plate structures", *Proceedings of the Annual Autumn Meeting of SNAK*, Sancheong, Gyeongsangnam-do, Korea.

Kwon, Y.B. and Hancock, G.J. (1991), "A nonlinear elastic spline finite strip analysis for thin-walled sections", *Thin Wall. Struct.*, **12**(4), 295-319.

Levy, S. (1943), "Large Deflection Theory of Curved Sheet", NACA TN 895.

Madenci, E. and Barut, A. (1994), "Pre- and postbuckling response of curved, thin, composite panels with cutouts under compression", *Int. J. Number. Method. Eng.*, **37**(9), 1499-1510.

Maeno, Y., Yamaguchi, H., Fujii, Y. and Yao, T. (2003), "Study on buckling/ultimate strength of bilge circle part and its contribution to ultimate hull girder strength", *J. Soc. Nav. Archit. Jpn.*, **194**, 171-178.

Maeno, Y., Yamaguchi, H., Fujii, Y. and Yao, T. (2004), "Buckling/plastic collapse behaviour and strength of bilge circle and its contribution to ultimate longitudinal strength of ship's hull girder", *Proceedings of Fourteenth International Offshore and Polar Engineering Conference*, Toulon, France, May.

Paik, J.K. and Thyamballi, A.K. (2003), *Ultimate Limit State Design of Steel-Plated Structures*, John Wiley & Sons, Chichester, West Sussex, England.

Paik, J.K., Lee, J.M. and Lee, D.H. (2003), "Ultimate strength of dented steel plates under axial compressive loads", *Int. J. Mech. Sci.*, **45**(3), 433-448.

Park, H.J., Cho, S.R., Chung, J.N. and Lee, D.B. (2005), "Ultimate strength analysis of curved stiffened shell of container bilge strake", *Proceedings of the Annual Autumn Meeting of SNAK*, Sancheong, Gyeongsangnam-do, Korea.

Park, J.S., Fujikubo, M., Iijima, K. and Yao, T. (2009), "Prediction of the secondary buckling strength and ultimate strength of cylindrically curved plate under axial compression", *Proceedings of the Nineteenth International Offshore and Polar Engineering Conference*, Osaka, Japan, June.

Park, J.S., Iijima, K. and Yao, T. (2008), "Characteristics of buckling and ultimate strength and collapse

behaviour of cylindrically curved plates subjected to axial compression", *Adv. Mat. Res.*, **33-37**, 1195-1200.

Smith, C.S., Davidson, P.C., Chapman, J.C. and Dowling, P.J. (1988), "Strength and stiffness of ships' plating under in-plane compression and tension", *Trans. RINA.,* **130**, 227-296.

Ueda, Y. and Yao, T. (1985), "The influence of complex initial deflection modes on the behavior and ultimate strength of rectangular plates in compression", *J. Constr. Steel. Res.*, **5**(4), 265-302.

Yumura, K., Katsura, S., Iijima, K. and Yao, T. (2005), "Simulation of buckling collapse behaviour of cylindrically curved plates under axial compression", *The Nineteenth Asian Technical Exchange and Advisory Meeting on Marine Structures*, Singapore, Republic of Singapore, December.